Monitoring Retinal Morphologic and Functional Changes in Mice Following Optic Nerve Crush

Yang Liu, Colleen M. McDowell, Zhang Zhang, Holly E. Tebow, Robert J. Wordinger, and Abbot F. Clark

North Texas Eye Research Institute and Department of Cell Biology and Immunology, University of North Texas Health Science Center, Fort Worth, Texas, United States

Correspondence: Abbot F. Clark, Department of Cell Biology and Immunology, North Texas Eye Research Institute, University of North Texas Health Science Center, 3500 Camp Bowie Boulevard, Fort Worth, TX 76107, USA; abe.clark@unthsc.edu.

Submitted: January 6, 2014
Accepted: May 2, 2014

Citation: Liu Y, McDowell CM, Zhang Z, Tebow HE, Wordinger RJ, Clark AF. Monitoring retinal morphologic and functional changes in mice following optic nerve crush. *Invest Ophthalmol Vis Sci*. 2014;55:3766–3774. DOI:10.1167/iovs.14-13895

Purpose. We characterized the morphologic and functional changes in optic nerve crushed mice and evaluated electroretinogram (ERG) responses as tools to monitor retinal ganglion cell (RGC) dysfunction.

Methods. We performed optic nerve crush (ONC) unilaterally in adult BALB/cJ mice. The neuronal loss in the RGC layer (GCL) and superior colliculus (SC) was determined by Nissl staining. Retinal thickness was assessed by spectral-domain optical coherence tomography (SD-OCT) imaging. Retinal function was determined by pattern ERG and full-field flash ERG. Responses of pattern ERG, positive scotopic threshold response (pSTR), scotopic oscillatory potentials (OPs), and photopic negative response (PhNR) were analyzed.

Results. The ONC induced progressive neuronal loss in GCL and contralateral SC starting from 7 and 28 days following ONC, respectively. A linear correlation was observed between combined thickness of nerve fiber layer (NFL), GCL, and inner plexiform layer (IPL) imaged by SD-OCT and cell numbers in GCL. Only half of the normal BALB/cJ mice exhibited pattern ERG response, which was smaller and later compared to C57BL/6J mice. The ONC reduced pattern ERG and pSTR, but the reduction of pattern ERG was earlier than pSTR, preceding the anatomical cell loss in the GCL. The PhNR and scotopic OPs were not affected by ONC.

Conclusions. The SD-OCT and ERG can be used to monitor noninvasively retinal morphologic and functional changes induced by ONC. Pattern ERG and pSTR are able to detect early RGC dysfunction, but pattern ERG exhibits higher sensitivity. Our results support the use of these tools in studies using the mouse ONC model.

Keywords: retinal ganglion cells, electroretinogram, optic nerve crush

Intraorbital optic nerve crush (ONC) induces apoptotic retinal ganglion cell (RGC) death.[1] The mouse ONC model has been used widely to investigate the mechanisms underlying axonal injury-induced RGC degeneration, and it also is a popular model in studies attempting to rescue RGCs and restore visual function. The number and the function of surviving RGCs are necessary parameters to determine the disease progression or treatment efficacy. To track structural and functional changes in the retina, noninvasive methods, such as spectral-domain optical coherence tomography (SD-OCT) and electroretinography (ERG), have been widely adopted.

Spectral-domain OCT specially designed for small animal imaging allows in vivo imaging of the mouse retina.[2,3] Quantitative morphologic information can be obtained from cross-sectional images. This approach has been used to measure retinal thickness in retinal degeneration. Retinal thinning determined by SD-OCT imaging in optic nerve crushed mouse retina has been reported[4]; however, the correlation between retinal thinning and progressive RGC loss has not been assessed to our knowledge.

Electroretinography is a useful tool to assess retinal function noninvasively. Depending on conditions of visual stimuli, ERG responses can be generated by various retinal cell types. Some flash ERG components have been reported to originate from the inner retina and are associated with RGC function. These include scotopic threshold response (STR), the most sensitive scotopic ERG component; oscillatory potentials (OPs), a series of high-frequency wavelets observed on the ascending edge of the ERG b-wave; and photopic negative response (PhNR), a negative response following the photopic b-wave.[5–8] Different from the full-field flash ERG, pattern ERG (PERG) is recorded under contrast reversal of pattern stimuli. The PERG response has been reported to diminish in RGC degenerations.[9–11] In most studies, ONC was used as a tool to separate the contributions of RGCs from the whole retina to the ERG response, and to that end, retinal functions were assessed at the later stage of injury. Therefore, whether the sensitivity of ERG is suitable for monitoring early RGC dysfunction must be evaluated.

In this study, we longitudinally examined the retinal structural and functional changes in adult albino mice following ONC. We evaluated the optic nerve injury-triggered neuronal loss in the ganglion cell layer (GCL) as well as the visual cortex, and assessed the correlation between SD-OCT imaged retinal thinning and progressive cell loss in the GCL. Furthermore, we compared the sensitivity of PERG and flash ERG components in detecting early RGC dysfunction. This study will help future investigations using these tools to monitor the progression of RGC degeneration and treatment efficacies in the ONC model as well as other models of RGC injury.

Materials and Methods

Animals

The C57BL/6J and BALB/cJ mice were purchased from Jackson Laboratory (Bar Harbor, ME, USA). Mice used in this study were 3- to 6-month-old females. All animals were handled in accordance with the ARVO Statement for the Use of Animals in Ophthalmic and Vision Research, using protocols approved and monitored by the University of North Texas Health Center Animal Care and Use Committee.

Mouse Model of ONC

Mice were anesthetized by intraperitoneal (IP) injection of ketamine and xylazine (100 and 10 mg/kg, respectively). The ONC was performed as described previously.[1] Briefly, the left optic nerve was exposed intraorbitally through a small window made between the surrounding muscles. The optic nerve was crushed under visualization approximately 1 mm behind the globe with self-closing forceps for 4 seconds.

Quantification of Cell Numbers in the GCL

Quantification of cell numbers in the GCL was performed from flat-mounted and Nissl-stained retinas. At 3 to 28 days after ONC, mice ($n = 8$–10 per time point) were euthanized, and the eyes were enucleated and fixed in 4% paraformaldehyde (Electron Microscopy Sciences, Hatfield, PA, USA) for 50 minutes. After fixation, retinas were carefully dissected, flat-mounted on "Superfrost" glass slides (Fischer Scientific, Pittsburgh, PA, USA), and Nissl-stained with 1% cresyl violet (Sigma-Aldrich, St. Louis, MO, USA) in 0.25% acetic acid for 30 to 45 seconds as described previously.[12] The stained retinas were dehydrated and then mounted for microscopic evaluation. Eight images of ×40 magnification were taken from peripheral and mid peripheral regions in four quadrants of each retina. Images were imported into Adobe Photoshop software (Adobe Systems, Inc., San Jose, CA, USA). The number of cells in a total of four equal sized fields (0.02 mm^2 retina area in total) from each image was counted. The number of cells presented in each retina was taken as the average of these counts. Cell counts were performed in a masked manner.

Quantification of Cell Numbers in Superior Colliculus (SC)

To identify the region in the SC innervated by RGC axons, mice were injected intravitreally with 2 μL of Cholera Toxin B-subunit (CTB) conjugated with AlexaFluor 488 (Invitrogen, Grand Island, NY, USA). At 48 hours after the injection, the mice were killed and brain coronal sections were imaged. Templates highlighting the region of fluorescence were prepared for future cell counting.[13] At designed time points after the ONC, mice ($n = 5$ per time point) were killed and brains were fixed in 10% neutral buffered formalin (Statlab, McKinney, TX, USA) overnight. Paraffin-embedded brains then were sectioned coronally, and stained with 0.04% cresyl violet (Electron Microscopy Sciences) in 0.3% acetic acid for 1 hour. Nissl-stained cells in the template regions from the same SC sections of each brain were counted in a masked matter.

SD-OCT Imaging and Analysis

The SD-OCT imaging was performed longitudinally before and up to 28 days ($n = 4$) after ONC using a Bioptigen ophthalmic imaging system (Bioptigen, Durham, NC, USA). Before imaging, mice were anesthetized with an intraperitoneal injection of ketamine (100 mg/kg) and xylazine (10 mg/kg), and pupils were dilated using 2.5% phenylephrine (Bausch & Lomb, Rochester, NY, USA). Corneas were kept moist during imaging with 2.5% hypromellose ophthalmic solution (Akorn, Lake Forest, IL, USA). Radial volume scans (centered on optic disc, diameter 1.2 mm) were performed. Each volume consisted of 100 B-scans with 1000 A-scans per B-scan. Data processing was performed with image analysis software (InVivoVue Clinic; Bioptigen). Four images (scans 1, 26, 51, and 76 at 0°, 45°, 90°, and 135° in en face image) were used for the retinal thickness measurement. For each selected image, two vertical calipers were placed on each side of the optic nerve head, 400 and 500 μm away from the center of the optic nerve head. The caliper defined the combined thickness of the nerve fiber layer (NFL), GCL, and inner plexiform layer (IPL). The combined thickness of NFL, GCL, and IPL of each retina was taken as the average of total eight measurements. The image analysis was performed in a masked manner.

PERG Recording

Pattern ERG was performed with a UTAS Visual Electrodiagnostic System (LKC, Gaithersburg, MD, USA), using DTL-plus electrodes. Mice were anesthetized with an IP injection of ketamine/xylazine/acepromazine (100/10/3 mg/kg). Anesthesia was maintained with ketamine (50 mg/kg) as needed. Each mouse was placed on a thermostatically controlled heating pad during the recording. Body temperature was monitored via a rectal thermometer and maintained at 37.0°C. The projection of the pupil was aligned to the center of the pattern monitor at a distance of 20 cm. The DTL-plus electrodes were placed gently on the lower part of the corneal surface without interfering with the vision. The cornea was kept moist with a thin layer of artificial tear ointment (Rugby Laboratories, Duluth, GA, USA). Reference and ground electrodes were stainless steel needles inserted under the skin of the back of the head and tail, respectively.

The pattern stimuli were displayed on an RGB monitor (model Dell M933S; Dell, Inc., Round Rock, TX, USA). Stimuli consisted of 0.05 cyl/deg horizontal black and white bars reversing at 1 Hz, presented at 100% contrast and average ambient room lighting mean luminance 100 cd/m^2. A total of 1800 responses was averaged.[14] The amplitude was measured from the baseline to the peak, and the latency was the time to the peak of the positive response. To compare PERG responses between different mouse strains, 12 pigmented eyes and 22 albino eyes were recorded. For PERG response following ONC, five mice were included.

Full Field Flash ERG Recording

Full field flash ERG was performed with the Handheld Multi-species-ElectroRetinoGraph (HMsERG) unit (Ocuscience, Kansas City, MO, USA), using thread electrodes. Mice were dark adapted overnight before the ERG recording. Isoflurane (Bulter Schein Animal Health, Dublin, OH, USA) inhalation anesthesia was maintained during the recording procedure. All the procedures were performed in a dark room with a dim red safe light as needed. Body temperature was monitored via a rectal probe and maintained at 37.0°C by a heating pad. Pupils were dilated with 2.5% phenylephrine ophthalmic eye drops. Thread electrodes were placed across the center of each cornea. The cornea was moistened with 2.5% hypromellose ophthalmic solution (Arkon, Lake Forest, IL, USA) covered with a 2.5-mm clear contact lens. The corresponding reference electrode was a stainless steel needle placed subcutaneously in the area below each eye. Another needle electrode, which served as ground electrode, was inserted into the skin of the

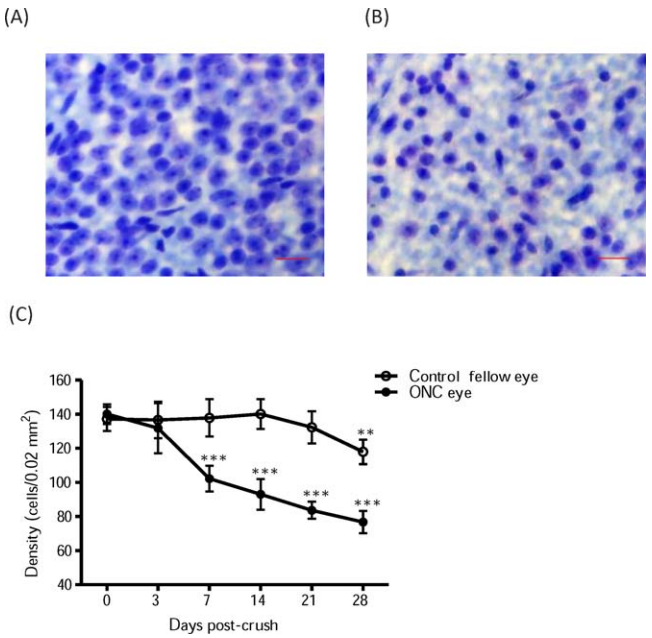

Figure 1. Cell loss in the GCL following ONC. (**A**) Nissl-stained retina from a mouse before ONC. (**B**) Nissl-stained retina from an ONC eye 28 days after injury. Each figure is representative of the midperipheral superior retina. The crushed eye showed dramatic loss of cells. *Scale bars*: 10 μm. (**C**) Graphic representation of cell loss in RGC layer after ONC. Starting 7 days after intraorbital ONC, the loss of RGCs was continuous, and cell number in the RGC layer was significantly lower in the crushed eyes. At 28 days post crush, there also was a significant cell loss in the GCL of the control fellow eyes. Each *data point* represents mean ± SD, $n = 8$ to 10. $^{**}P < 0.01$, $^{***}P < 0.001$ compared to the baseline.

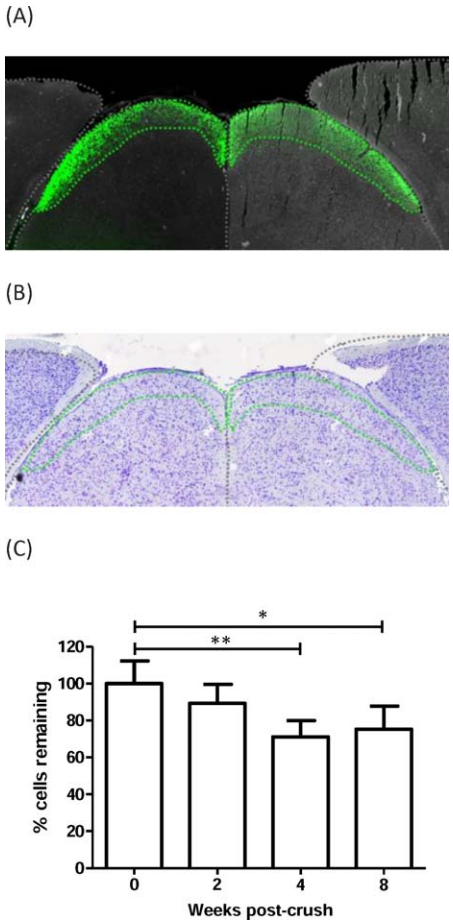

Figure 2. Cell loss in the SC following ONC. (**A**) The region in the SC innervated by RGC axons was identified by intravitreal injection with Cholera Toxin B-subunit conjugated with AlexaFluor 488. Templates highlighting the region with fluorescence were prepared for future cell count. (**B**) Quantification of cell numbers in SC. The ONC-induced cell loss in the SC was measured from Nissl-stained brain paraffin sections. Nissl-stained cells in the template regions of each brain were counted. (**C**) Graphic representation of cell loss in SC after ONC. Starting from 4 weeks after ONC, there were less cells remaining in the contralateral SC compared to the control group. Each *data point* represents the mean ± SD, $n = 5$. $^{*}P < 0.05$, $^{**}P < 0.01$ compared to the baseline.

tail. Bilateral ERG recording was performed from both eyes simultaneously.

The light stimuli were generated in a Ganzfeld doom with light emitting diodes (LED). The ERG responses were recorded by stimulating the retina with light intensities ranging between 3×10^{-5} cd·s·m^{-2} and 0.03 cd·s·m^{-2} for the scotopic test. Numbers of response averaged and interval between flashes were adjusted to the light intensity. For the dimmest stimulus, responses from 30 flashes with 2-second intervals were averaged. For the brightest stimulus, responses from four flashes with 10-second intervals were averaged. The mice were subjected to the light adaptation for 15 minutes after the scotopic ERG exams, and the background light intensity was 30 cd·s·m^{-2}. The light intensity for the photopic ERG test ranged between 0.01 and 25 cd·s·m^{-2}. Responses from 32 flashes with 0.5-second intervals were averaged. The effects of ONC on scotopic OPs were studied in a separate group of mice. The light intensities for OPs recording ranged from 0.1 to 25 cd·s·m^{-2}. Responses from four flashes with 10-second intervals were averaged for the dimmer stimuli. Response to the brightest stimulus was recorded only once.

The pSTRs ($n = 6$) were measured from the baseline to the positive peak of the waveform at the flash intensity of 3×10^{-5} cd·s·m^{-2}, and the PhNRs ($n = 6$) were measured from the baseline to the trough of the negative response following the positive b-wave at the flash intensity of 10 cd·s·m^{-2}. The OPs ($n = 6$) were extracted by digital filtering of the raw signal with the bandwidth of 100 to 300 Hz. Amplitudes of OPs were measured from the preceding trough to the peak of each individual OP.

Statistical Analysis

A 1-way ANOVA with Dunnett's posttest for multiple comparisons was used to compare the difference among multiple groups. Unpaired Student's *t*-test was used for the comparison between two groups. Correlation between the morphologic and functional measurements was assessed by Pearson's correlation coefficient. Results are presented as mean ± SD and the significant level was set at 0.05.

Results

Cell Loss in the Retina and SC Following ONC

To correlate the retinal functional changes to morphologic changes induced by optic nerve injury, we evaluated cell loss in the GCL 3 to 28 days following ONC (Fig. 1). A progressive cell loss started 7 days post crush in the GCL of the crushed eyes. Nissl-stained retinas showed 102 ± 4 cells/0.02 mm^2 before ONC and 56 ± 5 cells/0.02 mm^2 remaining at 28 days post

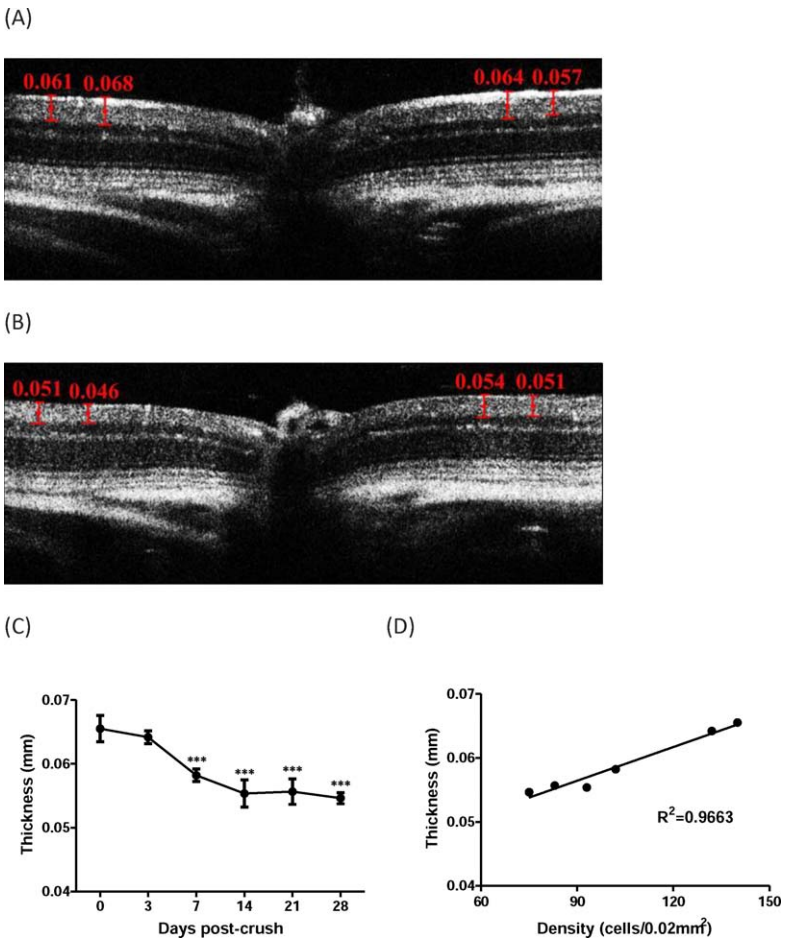

Figure 3. Thinning of retinal layers determined by SD-OCT. (**A**) Representative individual B-scan image (scan 1 at 0° in en face image) from a mouse before ONC. (**B**) Representative individual B-scan image (scan 1 at 0° in en face image) from a mouse 28 days after ONC. Two vertical calipers were placed on each side of the optic nerve head, 400 and 500 μm away from the center of the optic nerve head. The caliper defined the combined thickness (mm) of the NFL, GCL, and IPL. (**C**) Graphic representation of retinal thinning after ONC. Starting from 7 days after ONC, combined thickness of NFL, GCL, and IPL determined by SD-OCT imaging decreased. Each *data point* represents the mean ± SD, $n = 4$. $^{***}P < 0.001$ compared to the baseline. (**D**) Scatter plot showing a strong correlation between cell counts and measured retinal thickness. The cell counts of Nissl-stained retinas were plotted as the independent variable and the combined thickness of NFL, GCL, and IPL as the dependent viable. $R^2 = 0.9663$, $P < 0.001$.

ONC. In the mouse retina, 40% to 60% of the neurons in the RGC layer are ganglion cells.[15–17] Since ONC induces selective RGC death,[1,11] there were very few RGCs remaining 28 days after ONC. Unilateral ONC also induced cell death in the GCL of control fellow eyes, where there was approximately 20% cell loss detected at 28 days following ONC.

Since more than 90% of RGC axons target contralateral SC in albino mice,[18] we evaluated cell loss in SC 2 to 8 weeks following ONC. In contrast to the rapid cell death in the RGC layer, ONC induced cell loss in the contralateral SC in a more protracted manner. At 4 weeks after ONC, 28.9% ± 8.8% neuronal death was first detected in contralateral SC, no further decrease in cell numbers has been observed at 8 weeks following the crush (Fig. 2). We did not find significant cell loss in ipsilateral SC (data not shown).

Thinning of Retinal Layers Monitored by SD-OCT

To further evaluate ONC-induced morphologic changes in the retina, we performed longitudinal SD-OCT scanning before and 3 to 28 days following ONC. The combined thickness of NFL, GCL, and IPL before ONC was 65.5 ± 2.1 μm. These combined layers showed a progressive thinning from 7 through 28 days (54.6 ± 0.9 μm) post crush, which matched the time point of the first detected cell loss in the RGC layer (Figs. 3A–C). To evaluate the correlation between retinal thickness and cell loss in RGC layer, the actual counts of the Nissl-stained cells in RGC layer were plotted as an independent variable to the dependent measured thickness. A significant correlation between cell counts in the GCL and combined thickness of the NFL, GCL, and IPL was observed ($R^2 = 0.9663$, $P < 0.001$, Fig. 3D).

PERGs Following ONC

To study the effect of ONC on PERG waves, we performed baseline PERG recordings before the surgery. Only approximately half of the BALB/cJ mice tested were PERG responders; in contrast, all the tested C57BL/6J mice had PERG responses. We further compared the amplitudes and latencies of the PERG responses from C57BL/6J and BALB/cJ responder mice under the same recording conditions. Both strains showed a positive peak in response to the pattern stimuli (Fig. 4A). However, the responses of albino mice with detectable waveforms were smaller (5.9 ± 2.2 μV) and delayed (124 ± 12 ms) compared to pigmented mice (9.0 ± 2.9 μV and 69 ± 4 ms, Figs. 4B, 4C).

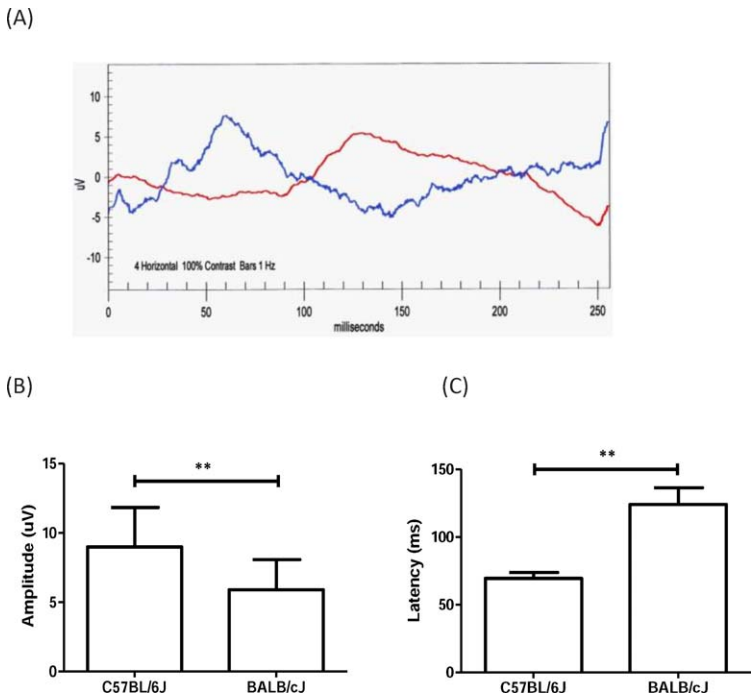

FIGURE 4. The PERGs in normal eyes of C57BL/6J and BALB/cJ mice. (**A**) Representative PERG traces recorded in a normal C57BL/6J (*blue line*) or BALB/cJ (*red line*) mouse in response to 0.05 cyl/deg gratings reversing in contrast at 1 Hz presented at 100% contrast. Both stains showed positive waves in response to pattern stimuli. However, only approximately 50% of recorded eyes of BALB/cJ mice had PERG responses. (**B**) Averaged PERG amplitudes of recordings from pigmented eyes (C57BL/6J) and albino eyes (BALB/cJ). (**C**) Averaged PERG latency of recordings from pigmented eyes and albino eyes. The PERGs from albino eyes were smaller and later than those from pigmented eyes. Each *data point* represents the mean ± SD, $n = 12$ pigmented eyes, 22 albino eyes. $^{**}P < 0.01$.

The ONC was performed on BALB/cJ PERG responders. Representative PERG traces recorded from a mouse before, and 3 and 7 days following ONC are displayed in Figure 5A. The PERGs were similar in waveform before and 3 days after crush. However, PERG amplitudes were significantly reduced 3 days after ONC ($P < 0.05$) and totally eliminated 7 days after ONC ($P < 0.001$, Fig. 5B).

Flash ERGs Following ONC

Scotopic ERGs were recorded before and 3 to 38 days after ONC. With very dim light flashes (3×10^{-5} cd·s·m^{-2}), STRs were elicited. As flash intensity increased, the recorded responses switched to scotopic b-waves and a-waves (Fig. 6A). The effects of ONC on pSTR were analyzed by measuring the amplitudes and latencies at flash intensity 3×10^{-5} cd·s·m^{-2}. The pSTR amplitude reduction was first detected 7 days after ONC, which was coincident with the first detected morphologic changes in the inner retina. At 28 days following ONC, pSTRs could still be elicited; the amplitudes decreased from the baseline level of 30.3 ± 9.4 to 13.6 ± 4.4 μV (Fig. 6). The latency of pSTR was not significantly delayed after ONC (data not shown).

Photopic responses were recorded with flash intensities ranging from 0.03 cd·s·m^{-2} to 25 cd·s·m^{-2}. Starting from 0.3 cd·s·m^{-2}, photopic b-waves were elicited. In response to stronger flash intensities, the amplitudes of b-waves and PhNRs increased, and the PhNR saturated at 10 cd·s·m^{-2} (Fig. 7A). We analyzed PhNRs at 10 cd·s·m^{-2}, and the results showed a trend

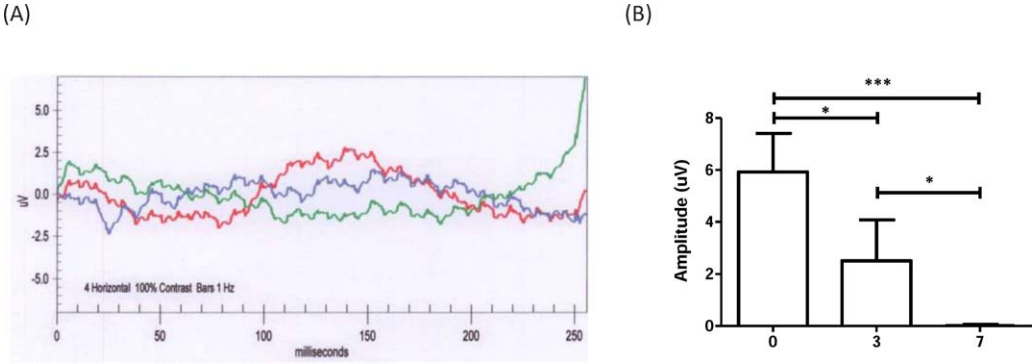

FIGURE 5. The PERGs were eliminated following ONC. (**A**) Representative PERGs before (*red line*), and 3 (*blue line*) and 7 (*green line*) days after ONC. (**B**) Averaged data of PERG amplitudes from recordings obtained before, and 3 and 7 days after ONC. The PERG amplitudes were significantly reduced 3 days after ONC and totally eliminated 7 days after ONC. Each *data point* represents the mean ± SD, $n = 5$. $^{*}P < 0.05$, $^{***}P < 0.001$ compared to the baseline.

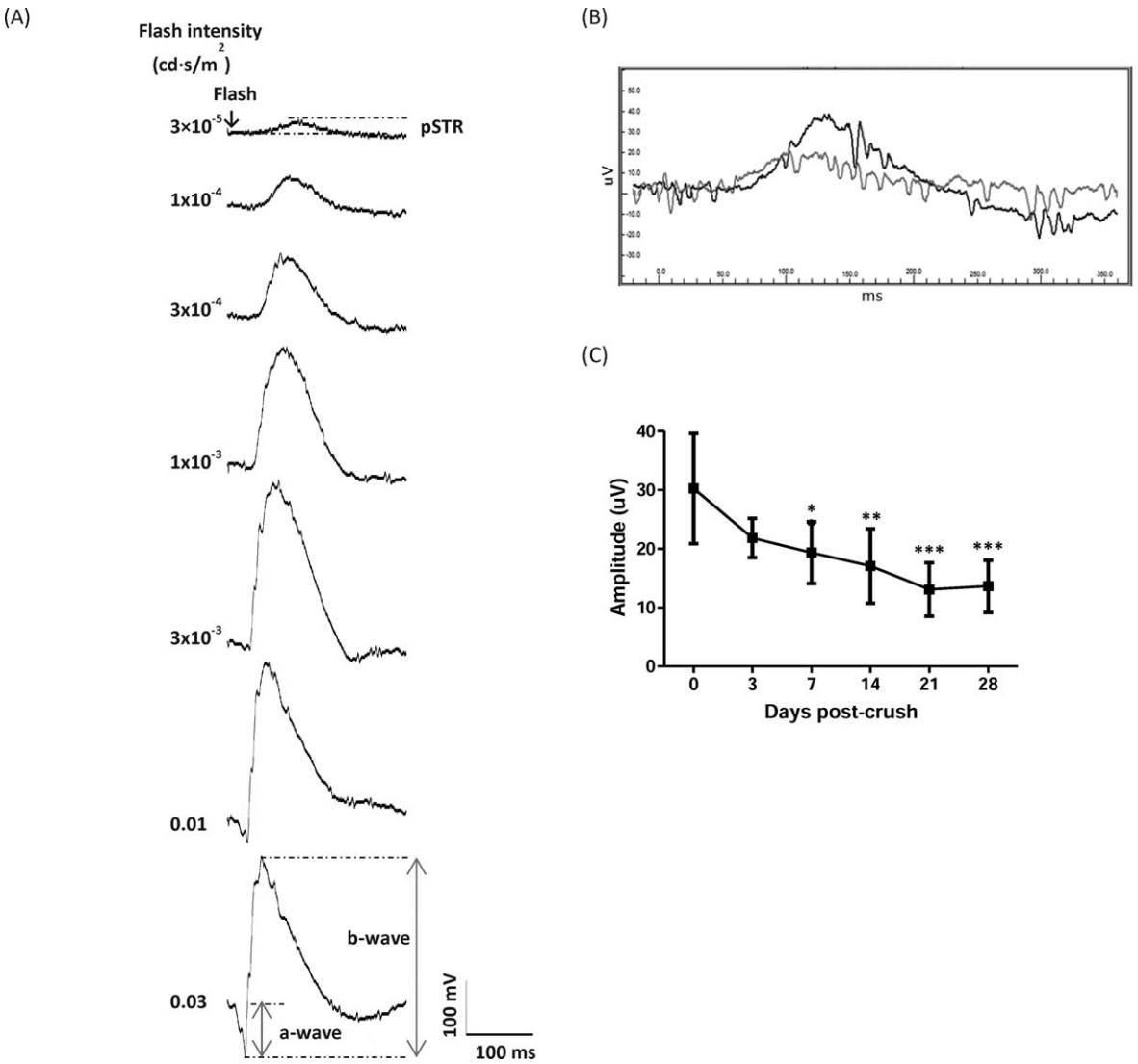

Figure 6. The pSTRs diminished following ONC. (**A**) Representative scotopic series in response to increasing flash intensity. The pSTR was elicited with very dim light stimuli, while scotopic b-waves and a-waves were recorded with stronger flash stimuli. The pSTR was measured from the baseline to the positive peak of the waveform. (**B**) Representative scotopic traces before (*black line*) and 28 days (*gray line*) after ONC. The amplitude of pSTR decreased, but the latency did not change after ONC. (**C**) Averaged data of pSTR amplitudes from recordings obtained before, and 3 through 28 days after ONC. The pSTR amplitudes were assessed at a flash intensity of 3×10^{-5} cd·s·m^{-2}. The ONC progressively reduced pSTR amplitudes starting from 7 days after ONC. Each *data point* represents the mean ± SD, $n = 6$. $^{*}P < 0.05$, $^{**}P < 0.01$, $^{***}P < 0.001$ compared to the baseline.

of decrease after ONC; however, the change of PhNR was not statistically significant (Fig. 7B).

Scotopic OPs were extracted from scotopic responses elicited with light intensities ranged from 0.1 to 25 cd·s·m^{-2}. Scotopic OPs from BALB/cJ mice contained 4 peaks. The predominant two peaks, OP2 and OP3, were analyzed. The ONC did not induce significant changes in OP amplitudes and latencies (data not shown).

Discussion

In this study, we characterized the structural and functional changes following intraorbital ONC in albino mice. Cell numbers in GCL and retinal thickness were used as indicators of morphologic damage to correlate with RGC functional loss. We found that optic nerve injury induces neuronal loss not only in the GCL, but also subsequently in the visual cortex. For monitoring RGC function, pattern and flash ERGs correlated with retinal morphologic changes, but PERG was able to detect RGC dysfunction before significant structural damage was evident. These findings have significant implications for future studies using these assessments to monitor RGC disease/injury progression and to evaluate treatment efficacy.

Nissl stain displays RGCs and displaced amacrine cells in the retina. Loss of RGCs following optic nerve injury has been well documented.[1,11,19,20] In contrast, to our knowledge the death of displaced amacrine cells after ONC has never been shown in adult animals. Therefore, we expect that the time course of RGC loss following ONC can be demonstrated using the Nissl stain. Total retinal thinning induced by ONC can be detected by SD-OCT imaging.[4,21] Camp et al.[22] demonstrated that combined thickness of NFL and IPL represents the cell loss in the GCL in Brn3b knockout mice. We measured the combined thickness of NFL, GCL, and IPL where the major structural degeneration occurs after ONC, and found that this

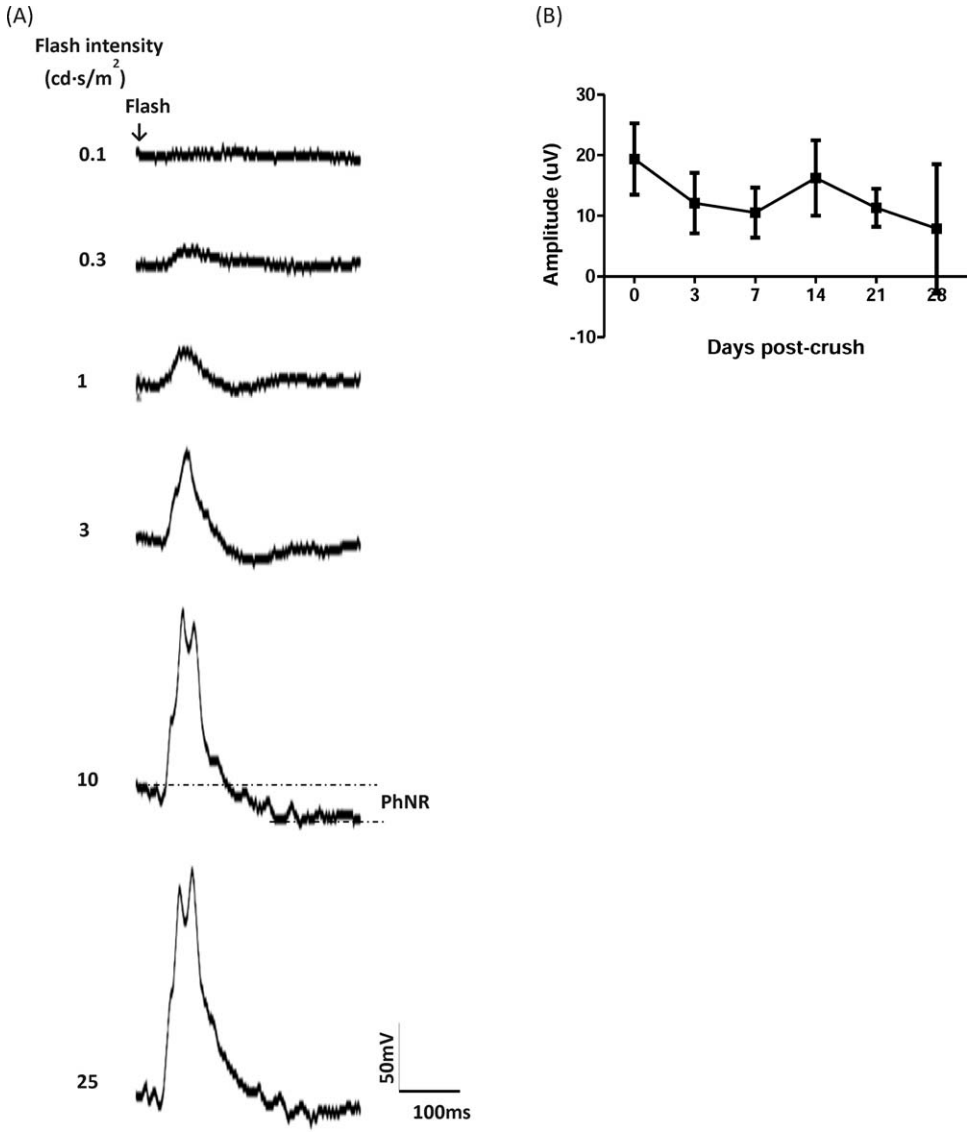

FIGURE 7. No significant reduction of PhNRs following ONC. (**A**) Representative photopic series in response to increasing flash intensity. Photopic b-waves were elicited starting from 0.3 cd·s·m^{-2}. The PhNR amplitudes increased in response to stronger flash intensities and saturated at flash intensity of 10 cd·s·m^{-2}. The response was measured from the baseline to the trough of the negative response following the b-wave. (**B**) Averaged data of PhNR amplitudes from recordings obtained before, and 3 through 28 days after ONC. The PhNR amplitudes were assessed at the flash intensity of 10 cd·s·m^{-2}. The change of PhNR was not statistically significant. Each *data point* represents the mean ± SD, $n = 6$.

combined thickness correlated with cell numbers in the GCL. This finding supported the validity of using noninvasive SD-OCT to monitor inner retinal thinning in the mouse ONC model.

Pattern ERG is a powerful tool for assessing RGC function in animal models that mimic glaucomatous retinopathy. The methodology of recording mouse PERG and changes of PERG following optic nerve injury in pigmented mice have been described in several studies. The elimination of PERG at late or advanced stage of these models is evident when RGC degeneration is obvious.[10,14,23,24] We showed that PERG reduction happened as early as 3 days after ONC, when cell loss in GCL was not significant. The time course of retinal gene expression changes following optic nerve injury has been described in a variety of studies.[25–28] The downregulation of normally-expressed RGC maker genes and upregulation of apoptotic genes occur before anatomical cell death. For example, Thy1 expression decreased within 24 hours after ONC.[29] Caspase 3 activation peaked at 48 hours after the injury.[25] The upregulation of caspase 11 was detected as early as 12 hours and lasted up to 7 days after the insult.[30] These cell death signals may contribute to the early retinal dysfunction preceding the anatomical RGC loss, which is indicated by reduction of PERG shown in our study.

In our study, we used BALB/cJ mice, since this strain is more susceptible to the optic nerve injury than other commonly used strains.[12] Visual defects have been reported in BALB/c strains.[31–33] We performed PERG prescreening and found that approximately half of tested BALB/cJ mice responded to pattern stimuli. In addition, the responders showed smaller and delayed responses compared to pigmented C57BL/6J mice. The albino mammals exhibited impaired ability of visual detection and pattern discrimination due to reduced photoreceptors and decreased ipsilateral projecting retinal fibers.[31,34,35] However, we did not find obvious pathologic changes in the retinas of these mice. In addition, all the tested

BALB/cJ mice had similar scotopic and photopic ERG responses, which indicated the PERG responders and nonresponders had similar outer retinal function. Therefore, the miswiring of RGC axons presumably accounts for the lack of responses to pattern stimuli in BALB/cJ mice. To our knowledge, this is the first report of PERG responses from albino mice. Our results suggested a prescreening procedure for studies using PERG monitoring of visual function in BALB/c mice.

Some flash ERG components have been shown to originate in the inner retina and indicate retinal functional changes following optic nerve injury.[8,36,37] In our study, we analyzed pSTR, PhNR, and scotopic OPs in BALB/cJ mice 3 through 28 days after ONC. Consistent with previous studies,[8,36,38] we found that pSTR decreased gradually as RGCs degenerated, and the time course of pSTR reduction matched that of cell loss in the GCL. Compared to PERG, pSTR is less sensitive. It did not detect functional loss until structural damage could be detected. The precise retinal origination of STR is not clear, and other retinal neurons, such as bipolar cells, also contribute to the mouse STR.[9] This may explain the lack of sensitivity of STR for monitoring RGC dysfunction. However, the STR is less challenging to record than PERG because it does not require optimized vision and has higher signal-to-noise ratio. The pSTR (from 30.3 $\pm$ 9.4 to 13.6 $\pm$ 4.4 μV) also provides larger dynamic range than PERG (from 5.9 $\pm$ 2.2 to 0 μV), which makes it more suitable for treatment efficacy evaluation. Thus, the pSTR may be considered as an alternative approach to monitor RGC function.

The PhNR is believed to originate from the inner retina and be associated with the damage of retinal function in human glaucoma.[39–42] Our data showed that, despite a trend of reduction, the change of PhNR was not statistically significant. The endpoint of our study was 28 days after ONC, and it is possible that significant PhNR loss may appear later; but a later time point will not serve the purpose of detecting early RGC dysfunction. The decline of PhNR has been reported previously in optic nerve transected rats.[37] However, the investigators did not address the time point of statistically significant reduction of PhNR in their study. In addition, different optic nerve trauma models and species adopted in different studies may account for the apparent discrepancy in experimental results. Similarly, we did not find significant changes of scotopic OPs after ONC at all recorded flash intensities, which is consistent with previous studies.[8]

The retinal cell counts revealed a significant cell loss in the contralateral eyes at 28 days after ONC. Unilateral ONC induces bilateral effects, including inflammatory response, altered gene expression profiles, and the loss of ipsilaterally projecting RGCs.[5,6,43–45] Our study provided further evidence of retinal degeneration in uninjured contralateral eyes. Future studies are needed to characterize the degenerated cells in the GCL of the contralateral retinas. We also found a significant cell loss in contralateral SC starting from 4 weeks after ONC. This is not unexpected, since anterograde axonal transport is blocked as early as 24 hours after ONC, and the blockade of axonal transport or action potentials leads to neuronal death in the targeted visual center in the brain.[46,47] These findings suggest that not only the neurons in the injured eye, but also those in the contralateral eye and the visual cortex should be considered as neuroprotective targets after optic nerve injury.

In summary, we demonstrated that the progressive loss of cells in the GCL is highly correlated with SD-OCT determination of inner retinal thickness after ONC. Decreases in PERG responses occur before the morphologic loss of RGCs, with pSTR loss later. Noninvasive monitoring of retinal structure and function will be very useful in further studies of mouse RGC injury.

Acknowledgments

The authors thank Robert Nickells, PhD, for technical assistance on ONC model.

Supported by United States Department of Defense Grant DoD-W81XWH-10-2-0003.

Disclosure: **Y. Liu**, None; **C.M. McDowell**, None; **Z. Zhang**, None; **H.E. Tebow**, None; **R.J. Wordinger**, None; **A.F. Clark**, None

References

1. Li Y, Schlamp CL, Nickells RW. Experimental induction of retinal ganglion cell death in adult mice. *Invest Ophthalmol Vis Sci*. 1999;40:1004–1008.
2. Gabriele ML, Ishikawa H, Schuman JS, et al. Reproducibility of spectral-domain optical coherence tomography total retinal thickness measurements in mice. *Invest Ophthalmol Vis Sci*. 2010;51:6519–6523.
3. Nakano N, Ikeda HO, Hangai M, et al. Longitudinal and simultaneous imaging of retinal ganglion cells and inner retinal layers in a mouse model of glaucoma induced by N-methyl-D-aspartate. *Invest Ophthalmol Vis Sci*. 2011;52:8754–8762.
4. Gabriele ML, Ishikawa H, Schuman JS, et al. Optic nerve crush mice followed longitudinally with spectral domain optical coherence tomography. *Invest Ophthalmol Vis Sci*. 2011;52:2250–2254.
5. Panagis L, Thanos S, Fischer D, Dermon CR. Unilateral optic nerve crush induces bilateral retinal glial cell proliferation. *Eur J Neurosci*. 2005;21:2305–2309.
6. Macharadze T, Goldschmidt J, Marunde M, et al. Interretinal transduction of injury signals after unilateral optic nerve crush. *Neuroreport*. 2009;20:301–305.
7. Ferreri G, Buceti R, Ferreri FM, Roszkowska AM. Postural modifications of the oscillatory potentials of the electroretinogram in primary open-angle glaucoma. *Ophthalmologica*. 2002;216:22–26.
8. Bui BV, Fortune B. Ganglion cell contributions to the rat full-field electroretinogram. *J Physiol*. 2004;555:153–173.
9. Saszik SM, Robson JG, Frishman LJ. The scotopic threshold response of the dark-adapted electroretinogram of the mouse. *J Physiol*. 2002;543:899–916.
10. Miura G, Wang MH, Ivers KM, Frishman LJ. Retinal pathway origins of the pattern ERG of the mouse. *Exp Eye Res*. 2009;89:49–62.
11. Humphrey MF. A morphometric study of the retinal ganglion cell response to optic nerve severance in the frog Rana pipiens. *J Neurocytol*. 1988;17:293–304.
12. Li Y, Semaan SJ, Schlamp CL, Nickells RW. Dominant inheritance of retinal ganglion cell resistance to optic nerve crush in mice. *BMC Neurosci*. 2007;8:19.
13. McDowell CM, Luan T, Zhang Z, et al. Mutant human myocilin induces strain specific differences in ocular hypertension and optic nerve damage in mice. *Exp Eye Res*. 2012;100:65–72.
14. Porciatti V, Saleh M, Nagaraju M. The pattern electroretinogram as a tool to monitor progressive retinal ganglion cell dysfunction in the DBA/2J mouse model of glaucoma. *Invest Ophthalmol Vis Sci*. 2007;48:745–751.
15. Williams RW, Strom RC, Rice DS, Goldowitz D. Genetic and environmental control of variation in retinal ganglion cell number in mice. *J Neurosci*. 1996;16:7193–7205.
16. Jeon CJ, Strettoi E, Masland RH. The major cell populations of the mouse retina. *J Neurosci*. 1998;18:8936–8946.
17. Schlamp CL, Montgomery AD, Mac Nair CE, Schuart C, Willmer DJ, Nickells RW. Evaluation of the percentage of ganglion cells in the ganglion cell layer of the rodent retina. *Mol Vis*. 2013;19:1387–1396.

18. Drager UC, Olsen JF. Origins of crossed and uncrossed retinal projections in pigmented and albino mice. *J Comp Neurol*. 1980;191:383–412.
19. Villegas-Perez MP, Vidal-Sanz M, Rasminsky M, Bray GM, Aguayo AJ. Rapid and protracted phases of retinal ganglion cell loss follow axotomy in the optic nerve of adult rats. *J Neurobiol*. 1993;24:23–36.
20. Takeda M, Kato H, Takamiya A, Yoshida A, Kiyama H. Injury-specific expression of activating transcription factor-3 in retinal ganglion cells and its colocalized expression with phosphorylated c-Jun. *Invest Ophthalmol Vis Sci*. 2000;41:2412–2421.
21. Chauhan BC, Stevens KT, Levesque JM, et al. Longitudinal in vivo imaging of retinal ganglion cells and retinal thickness changes following optic nerve injury in mice. *PLoS One*. 2012;7:e40352.
22. Camp AS, Ruggeri M, Munguba GC, et al. Structural correlation between the nerve fiber layer and retinal ganglion cell loss in mice with targeted disruption of the Brn3b gene. *Invest Ophthalmol Vis Sci*. 2011;52:5226–5232.
23. Porciatti V, Pizzorusso T, Cenni MC, Maffei L. The visual response of retinal ganglion cells is not altered by optic nerve transection in transgenic mice overexpressing Bcl-2. *Proc Natl Acad Sci U S A*. 1996;93:14955–14959.
24. Porciatti V. The mouse pattern electroretinogram. *Doc Ophthalmol*. 2007;115:145–153.
25. Agudo M, Perez-Marin MC, Lonngren U, et al. Time course profiling of the retinal transcriptome after optic nerve transection and optic nerve crush. *Mol Vis*. 2008;14:1050–1063.
26. Templeton JP, Freeman NE, Nickerson JM, et al. Innate immune network in the retina activated by optic nerve crush. *Invest Ophthalmol Vis Sci*. 2013;54:2599–2606.
27. Yang Z, Quigley HA, Pease ME, et al. Changes in gene expression in experimental glaucoma and optic nerve transection: the equilibrium between protective and detrimental mechanisms. *Invest Ophthalmol Vis Sci*. 2007;48:5539–5548.
28. Levkovitch-Verbin H, Dardik R, Vander S, Nisgav Y, Kalev-Landoy M, Melamed S. Experimental glaucoma and optic nerve transection induce simultaneous upregulation of proapoptotic and prosurvival genes. *Invest Ophthalmol Vis Sci*. 2006;47:2491–2497.
29. Schlamp CL, Johnson EC, Li Y, Morrison JC, Nickells RW. Changes in Thy1 gene expression associated with damaged retinal ganglion cells. *Mol Vis*. 2001;7:192–201.
30. Agudo M, Perez-Marin MC, Sobrado-Calvo P, et al. Immediate upregulation of proteins belonging to different branches of the apoptotic cascade in the retina after optic nerve transection and optic nerve crush. *Invest Ophthalmol Vis Sci*. 2009;50:424–431.
31. Wong AA, Brown RE. Visual detection, pattern discrimination and visual acuity in 14 strains of mice. *Genes Brain Behav*. 2006;5:389–403.
32. Yeritsyan N, Lehmann K, Puk O, Graw J, Lowel S. Visual capabilities and cortical maps in BALB/c mice. *Eur J Neurosci*. 2012;36:2801–2811.
33. Brown RE, Wong AA. The influence of visual ability on learning and memory performance in 13 strains of mice. *Learn Mem*. 2007;14:134–144.
34. Rachel RA, Dolen G, Hayes NL, et al. Spatiotemporal features of early neuronogenesis differ in wild-type and albino mouse retina. *J Neurosci*. 2002;22:4249–4263.
35. Rebsam A, Bhansali P, Mason CA. Eye-specific projections of retinogeniculate axons are altered in albino mice. *J Neurosci*. 2012;32:4821–4826.
36. Alarcon-Martinez L, Aviles-Trigueros M, Galindo-Romero C, et al. ERG changes in albino and pigmented mice after optic nerve transection. *Vision Res*. 2010;50:2176–2187.
37. Li B, Barnes GE, Holt WF. The decline of the photopic negative response (PhNR) in the rat after optic nerve transection. *Doc Ophthalmol*. 2005;111:23–31.
38. Alarcon-Martinez L, de la Villa P, Aviles-Trigueros M, Blanco R, Villegas-Perez MP, Vidal-Sanz M. Short and long term axotomy-induced ERG changes in albino and pigmented rats. *Mol Vis*. 2009;15:2373–2383.
39. Viswanathan S, Frishman LJ, Robson JG, Harwerth RS, Smith EL III. The photopic negative response of the macaque electroretinogram: reduction by experimental glaucoma. *Invest Ophthalmol Vis Sci*. 1999;40:1124–1136.
40. Colotto A, Falsini B, Salgarello T, Iarossi G, Galan ME, Scullica L. Photopic negative response of the human ERG: losses associated with glaucomatous damage. *Invest Ophthalmol Vis Sci*. 2000;41:2205–2211.
41. Viswanathan S, Frishman LJ, Robson JG. The uniform field and pattern ERG in macaques with experimental glaucoma: removal of spiking activity. *Invest Ophthalmol Vis Sci*. 2000;41:2797–2810.
42. North RV, Jones AL, Drasdo N, Wild JM, Morgan JE. Electrophysiological evidence of early functional damage in glaucoma and ocular hypertension. *Invest Ophthalmol Vis Sci*. 2010;51:1216–1222.
43. Bodeutsch N, Siebert H, Dermon C, Thanos S. Unilateral injury to the adult rat optic nerve causes multiple cellular responses in the contralateral site. *J Neurobiol*. 1999;38:116–128.
44. Ananthakrishnan L, Gervasi C, Szaro BG. Dynamic regulation of middle neurofilament RNA pools during optic nerve regeneration. *Neuroscience*. 2008;153:144–153.
45. Lehmann U, Heuss ND, McPherson SW, Roehrich H, Gregerson DS. Dendritic cells are early responders to retinal injury. *Neurobiol Dis*. 2010;40:177–184.
46. Thuen M, Singstad TE, Pedersen TB, et al. Manganese-enhanced MRI of the optic visual pathway and optic nerve injury in adult rats. *J Magn Reson Imaging*. 2005;22:492–500.
47. Catsicas M, Pequignot Y, Clarke PG. Rapid onset of neuronal death induced by blockade of either axoplasmic transport or action potentials in afferent fibers during brain development. *J Neurosci*. 1992;12:4642–4650.

Investigative Ophthalmology & Visual Science